# Trap distribution for charge carriers in poly(paraphenylene vinylene) (PPV) and its substituted derivative DPOP-PPV

H. Meyer and D. Haarer
*Universität Bayreuth, LS EP IV and BIMF, D-95440 Bayreuth, Germany*

H. Naarmann
*BASF AG, D-ZK Geb. B1, D-67056 Ludwigshafen, Germany*

H. H. Hörhold
*Universität Jena, 07745 Jena, Germany*

(Received 23 January 1995; revised manuscript received 9 March 1995)

In this paper, we present measurements of the charge-carrier transport in the conjugated polymer poly(paraphenylene vinylene) (PPV) and its substituted derivative poly(1,4-phenylene-1,2-diphenoxyphenyl vinylene) (DPOP-PPV) by using the time-of-flight technique. A method for evaluating the experiments, based on Fourier transform techniques, is presented to calculate the density of localized states from the measured photocurrent within a multiple trapping model. The transport properties of DPOP-PPV can be described by a conventional hopping mechanism, where nearly every monomer acts as a trap. At room temperature, the effective mobility for holes in DPOP-PPV is in the range of $10^{-4}$ $cm^2/V\,s$, whereas for PPV, a value of less than $10^{-8}$ $cm^2/V\,s$ can be estimated.

## I. INTRODUCTION

Due to their electronic structure, conjugated polymers offer, in principle, a large area of possible applications (for reviews see, e.g., Refs. 1,2). In particular, the discovery of electroluminescence in poly(paraphenylene vinylene) (PPV) (Ref. 3) has stimulated recent work in this area.[4–9] For most technical applications, charge-carrier transport is one of the most important aspects of the device performance. In this paper, we report measurements of the charge transport properties of PPV and its substituted derivative poly(1,4-phenylene-1,2-diphenoxyphenyl vinylene) (DPOP-PPV) (Fig. 1) by using a standard time-of-flight (TOF) technique.

After describing experimental details in Sec. II, we will present in Sec. III a method for the numerical calculation of the density of localized states from the measured photocurrents. In Sec. IV, a short description of the numerical procedure is given in conjunction with a numerical test for the reliability of the evaluation algorithm. The results for DPOP-PPV and PPV will be discussed in Sec. V.

## II. EXPERIMENT

The photoconductivity data were obtained by the time-of-flight (TOF) technique. Since the details of our experimental procedures have been discussed elsewhere,[10] we will give only a short description of the method and of the experimental setup.

In a TOF experiment, the sample with a typical thickness of 10 $\mu$m is sandwiched between two electrodes. Electron-hole pairs are generated by a strongly absorbed laser pulse, which is irradiated through one of the (semitransparent) electrodes. For our experiments, we used the frequency tripled output of a Nd:YAG (yttrium aluminum garnet) laser Quantel YG501, with a pulse duration of 35 ps at a wavelength of 355 nm. At this wavelength the penetration depth for both, PPV and DPOP-PPV, is less than 5% of the sample thickness, and, hence, charges are only produced in a thin layer close to the illuminated surface.

The electron-hole pairs are separated by an externally applied electrical field. One species of carriers recombines immediately at the illuminated electrode, while the oppositely charged carriers drift across the sample, giving rise to a time-dependent photocurrent.

In the case of DPOP-PPV, the films with a thickness of about 4 $\mu$m were cast on Au-coated glass substrates from a 20 wt % solution in toluene by using a doctor blade technique.[10] After casting, the films were dried in vacuum for 4 h at 330 K to remove any residual solvent. Finally, the second Au electrode with an optical transmission of approximately 10% was vacuum deposited on top of the films.

The PPV films were cast from a sulfonium salt precursor solution[11] and converted to PPV by subsequent heating in vacuum ($p \approx 10^{-5}$ mbar) at 590 K for several hours. After elimination, the typical film thickness was about 7 $\mu$m. Elemental analysis shows that the residual

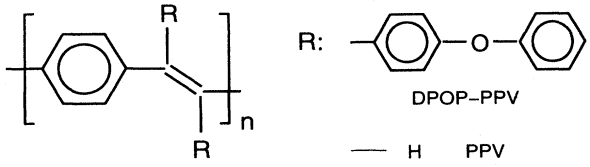


FIG. 1. Chemical structure of PPV and DPOP-PPV.

 

chlorine content after elimination depends upon the elimination temperature. By raising the elimination temperature from 530 to 590 K, the chlorine content drops from 6.03 wt % to 1.59 wt %. Simultaneously, the sulfur content drops from 0.69 wt % to 0.47 wt %. We found that changing the elimination temperatures and the elimination times did not cause any measurable changes in the photoconducting properties.

All measurements were performed either in vacuum ($p < 10^{-5}$ mbar) or in a He atmosphere. In the case of PPV, however, careful removal of oxygen is necessary to reduce the dark current. This was accomplished by heating the sample in vacuum to 490 K. After two days, the residual dark conductivity at room temperature has been reduced by roughly three orders of magnitude to a typical value of $5\times10^{-16}$ S/cm at an electrical field of $1.4\times10^{5}$ V/cm. This corresponds to a dark current of less than 1 nA.

We varied the temperature of the heat treatment between 420 and 490 K and found no differences in the photoconducting properties. Therefore, we conclude that no significant structural changes have been induced by the heat treatment. For the DPOP-PPV samples, heating was not required, since this material does not show self-doping by oxygen and the measured dark conductivities were in the range of $10^{-15}$ S/cm.

During the measurements, care was taken to avoid space-charge accumulation, due to high excitation intensities. In all cases, the total amount of generated photocharges was less than 10% of the product $CU$, where $C$ denotes the capacitance of the sample and $U$ the externally applied voltage. For the same reason, the waiting time between two excitations was kept long enough (typically some minutes) to ensure that almost all charge carriers from previous measurements had been swept out of the sample by the applied electrical field.

The photocurrents were either monitored with a two channel high-speed voltmeter (Keithley 1994 A) or with a transient recorder (Tektronix AD 7912 with plug-in 7A16B or 7A24) after proper preamplification. In the time range longer than 1 $\mu$s, all data were monitored with a single shot technique, while for shorter times the data were collected from typically three measurements at different time scales.

## III. CALCULATION OF TRAP DISTRIBUTIONS

In this section, we will present a method for calculating the trap distributions for charge carriers from the measured photocurrents in the TOF experiment. The analysis is based on the work of Oheda[12] and Brüggemann *et al.*[13] for the case of a transient photocurrent decay (TPC) experiment, either with a harmonically modulated excitation source[12,13] or with a pulsed excitation.[14]

We start with the well-known equations describing the trap controlled charge transport in the framework of the multiple trapping model,[15]

$$\frac{\partial}{\partial t}p(x,t)=f(x,t)-\int_0^{\epsilon_{fp}}\frac{\partial}{\partial t}m(x,t,\epsilon)d\epsilon - \frac{d}{t_{\mathrm{mic}}}\frac{\partial}{\partial x}p(x,t)\ , \tag{1a}$$

$$\frac{\partial}{\partial t}m(x,t,\epsilon)=p(x,t)\omega_c(\epsilon)-r(\epsilon)m(x,t,\epsilon)\ , \tag{1b}$$

$$r(\epsilon)=r_0 e^{-\epsilon/k_B T}\ . \tag{1c}$$

The definition of the above quantities is as follows.

$p(x,t)$: charge-carrier concentration in transport states.

$f(x,t)$: charge-carrier generation rate.

$t_{\mathrm{mic}}$: microscopic transit time of charge carriers in transport states.

$\epsilon$: trap depth, measured from mobility edge.

$\epsilon_{fp}$: quasi-Fermi-energy.

$m(x,t,\epsilon)d\epsilon$: concentration of charge carriers in traps of a depth between $\epsilon$ and $\epsilon+d\epsilon$.

$\omega_c(\epsilon)d\epsilon$: capture rate into traps with traps between $\epsilon$ and $\epsilon+d\epsilon$.

$r(\epsilon)$: thermal release rate from traps at depth $\epsilon$.

$r_0$: attempt-to-escape frequency.

$d$: sample thickness.

Here, the local carrier concentrations have already been integrated over the sample area; therefore, they have the dimension of a reciprocal length ($x=l/d$, $l$ is the spatial coordinate).

Equations (1a)–(1c) are commonly solved by a Laplace transform.[15,16] The disadvantage of this method is, however, that the calculation of the capture rates $\omega_c d\epsilon$ as a function of energy also requires an inverse Laplace transform,[16] which is known to be numerically problematic.

In the following, we will first consider the case of a harmonically modulated charge-carrier generation by a strongly absorbed light source, which is analogous to the modulated photocurrent technique (see, e.g., Refs. 12,13). In this case, the generation term in Eq. (1a) takes the form

$$f(x,t)=\frac{1}{d}(f_0+f_1 e^{-i\omega t})\delta(x-0)\ , \tag{2}$$

where the constant term $f_0$ has been introduced to avoid negative intensities of the excitation source. In the case of a TOF experiment, the dark current of the sample takes the role of $f_0$ and thus determines the quasi-Fermi-level $\epsilon_{fp}$ via the relation[12,17]

$$\frac{f_0 t_{\mathrm{mic}}}{V}=N_c e^{-\epsilon_{fp}/k_B T} \tag{3}$$

($V$ is the sample volume, $N_c$ is the effective density of states at the mobility edge). It will be shown later that for our measurements, the quasi-Fermi-level, which can be calculated using Eq. (3), is far removed from those trap levels, which control the transport properties. Hence, trap filling effects, due to the dark current, can be neglected.

The ansatz for the charge-carrier concentrations in the transport states and the traps reads

$$p(x,t)=\frac{1}{d}[p_0+g(x)e^{-i\omega t}]\sigma(x-0)\ , \tag{4}$$

$$m(x,t,\epsilon)=\frac{1}{d}[m_0+h(x)e^{-i\omega t}]\sigma(x-0)\ , \tag{5}$$

where $\sigma(x)$ denotes the unit step function. A straightforward calculation yields

$$h(x)=\frac{\omega_c(\epsilon)}{r(\epsilon)-i\omega}g(x) \tag{6}$$

and leads to a differential equation for the oscillating component $g(x)$ of the charge-carrier concentration of the following form:

$$\left[\delta(x)-i\omega t_{\rm mic}\left[1+\int_0^{\epsilon_{fp}}\frac{\omega_c(\epsilon)d\epsilon}{r(\epsilon)-i\omega}\right]\sigma(x)\right]g(x) +\sigma(x)\frac{\partial}{\partial x}g(x)=f_1 t_{\rm mic}\delta(x)\ . \tag{7}$$

Equation (7) can be solved by an analytical Laplace transform to give

$$g(x)=f_1 t_{\rm mic}e^{[-a(\omega)+ib(\omega)]x}\ , \tag{8}$$

$$a(\omega)=t_{\rm mic}\int_0^{\epsilon_{fp}}\frac{\omega^2\omega_c(\epsilon)}{r^2(\epsilon)+\omega^2}d\epsilon\ , \tag{9}$$

$$b(\omega)=\omega t_{\rm mic}\left[1+\int_0^{\epsilon_{fp}}\frac{\omega_c(\epsilon)r(\epsilon)}{r^2(\epsilon)+\omega^2}d\epsilon\right]\ . \tag{10}$$

By integrating Eq. (8) over the sample thickness, the oscillating component of the photocurrent $I(\omega)$ can be determined as

$$I(\omega)=Q_{\rm ges}\frac{1-e^{-a+ib}}{a-ib}\ , \tag{11}$$

with $Q_{\rm ges}=ef_1t_{\rm mic}$.

For the sake of convenience, the frequency dependence of $a$ and $b$ will, in the following, be carried explicitly only when necessary.

Since the expression in Eq. (11) is nothing else than a transfer function, $I(\omega)$ is identical to the Fourier transform of the photocurrent after pulsed excitation.[14]

Rewriting Eq. (11) yields for the absolute value and the phase shift $\tan\phi=\mathrm{Im}(I)/\mathrm{Re}(I)$,

$$|I(\omega)|=Q_{\rm ges}\left[\frac{1+e^{-2a}-2e^{-a}\cos b}{a^2+b^2}\right]^{1/2}\ , \tag{12a}$$

$$\tan\phi=\frac{b-e^{-a}(a\sin b-b\cos b)}{a+e^{-a}(b\sin b-a\cos b)}\ . \tag{12b}$$

Following Refs. 12 and 18, a demarcation energy $\epsilon_\omega$, at which the thermal release rate coincides with the modulation frequency of the excitation source, can be defined by the relation

$$\omega=r_0e^{-\epsilon_\omega/k_BT}\ . \tag{13}$$

For convenience, the release rate $\omega$ and the corresponding trap depth $\epsilon_\omega$ will, in the following, be used synonymously.

As can be seen from Eqs. (9) and (10), the quantities $a$ and $b$ are convolutions of the capture rates $\omega_c$ with the functions

$$g_1(z)=\frac{e^{2z}}{1+e^{2z}}\ , \tag{14a}$$

$$g_2(z)=\frac{e^{z}}{1+e^{2z}}\ , \tag{14b}$$

with

$$z=(\epsilon-\epsilon_\omega)/k_BT\ . \tag{14c}$$

In the limit $\epsilon_{fp}-\epsilon\gg k_BT$, Eqs. (14a) and (14b) are identical with the corresponding equations of Ref. 12. Therefore, $g_1$ and $g_2$ can be approximated by[12,13]

$$g_1(\epsilon,\omega)\approx\sigma(\epsilon-\epsilon_\omega)\ , \tag{15a}$$

$$g_2(\epsilon,\omega)\approx\frac{\pi}{2}k_BT\delta(\epsilon-\epsilon_\omega)\ , \tag{15b}$$

which limits the energy resolution of the method to $k_BT$. Equations (9) and (10) can now be rewritten to give

$$a(\omega)=t_{\rm mic}\int_{\epsilon_\omega}^{\epsilon_{fp}}\omega_c(\epsilon)d\epsilon\ , \tag{16}$$

$$b(\omega)=t_{\rm mic}\left[\omega+\frac{\pi}{2}k_BT\omega_c(\epsilon_\omega)\right]\ . \tag{17}$$

According to Eq. (16), $a(\omega)$ yields the number of capture events in traps deeper than $\epsilon_\omega$, which a charge-carrier experiences during the drift through the sample.

It will be shown later, that for high frequencies $a(\omega)$ is of the order of $10^4$. Therefore, Eqs. (12a) and (12b) can be rewritten as

$$|I(\omega)|=Q_{\rm ges}\frac{1}{\sqrt{a^2+b^2}}\ , \tag{18a}$$

$$\tan\phi=\frac{b}{a}\ , \tag{18b}$$

in the limit of $a\gg1$. Just as in the case of the TPC experiment,[13] the density of capture rates $\omega_c$ can then be calculated to be

$$\omega_c(\epsilon_\omega)=\frac{2}{\pi k_BT}\left[\frac{Q_{\rm ges}}{t_{\rm mic}}\frac{\sin\phi}{|I(\omega)|}-\omega\right]\ , \tag{19}$$

where $I(\omega)$ stands for the Fourier transform of the photocurrent. The phase shift $\phi$ is defined by the relation

$$\phi=\tan^{-1}\left[\frac{\mathrm{Im}I(\omega)}{\mathrm{Re}I(\omega)}\right]\ . \tag{20}$$

The fact that the equations for the density of capture rates are identical for both TOF and TPC methods can be understood on a qualitative base. In the case of the TOF experiment, the transport is dominated by traps for $a(\omega)\gg1$. Therefore, the effect of the absorbing counter electrode can be neglected and the situation is equivalent to that of the TPC method.

In the low-frequency regime, where the transport is dominated by traps, which, on the average, are visited

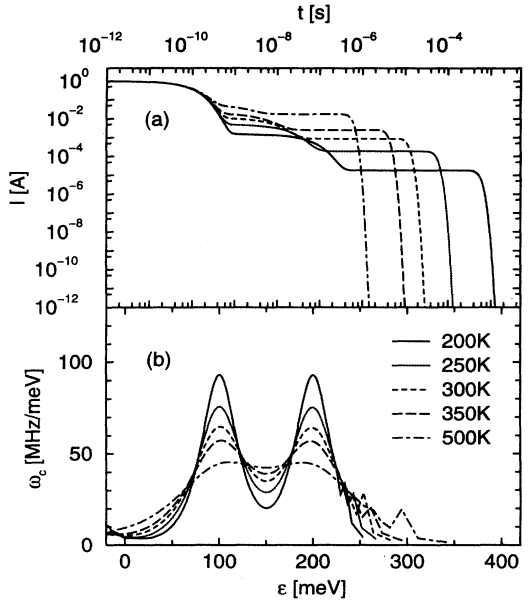


FIG. 2. (a) Calculated photocurrent for different temperatures, two discrete trap levels of equal density at 100 and 200 meV; (b) calculated density of capture rates $\omega_c$, broadening due to approximations (16) and (17); $r_0=10^{10}\ s^{-1}$, $t_{mic}=10^{-8}$ s.

less than once, the real and imaginary part of $I(\omega)$ can be expanded to second order in $a$ and $b$ to give [for definition of $a$ and $b$ see Eqs. (16) and (17)]

$$\frac{\mathrm{Re}I(\omega)}{Q_{ges}}=1\ , \tag{21}$$

$$\frac{\mathrm{Im}I(\omega)}{Q_{ges}}=\frac{b}{2}\ . \tag{22}$$

From Eqs. (22) and (17), the density of capture rates is then given by

$$\omega_c(\epsilon_\omega)=\frac{2}{\pi k_B T}\left[\frac{2}{Q_{ges}t_{mic}}\mathrm{Im}I(\omega)-\omega\right] \tag{23}$$

($a\ll 1$). In this case, all traps, which are relevant for the transport properties, are in thermal equilibrium and the influence of the counter electrode becomes important. Therefore, the results of both methods cannot be compared directly.

## IV. NUMERICAL TESTS

Since the TOF data cover roughly ten decades in time, a straightforward fast Fourier transform algorithm is impractical for computing the spectrum of the photocurrent. We, therefore, use the method described by Main *et al.*[14] In brief, the real and imaginary part of the Fourier transform are calculated by simple numerical integration from

$$\mathrm{Re}I(\omega_n)=\sum_{i=0}^{N_n-1}\Delta t_i I(t_i)\cos(\omega_n t_i)\ , \tag{24a}$$

$$\mathrm{Im}I(\omega_n)=\sum_{i=0}^{N_n-1}\Delta t_i I(t_i)\sin(\omega_n t_i)\ , \tag{24b}$$

with $\Delta t_i=\frac{1}{2}(t_{i+1}-t_{i-1})$. For short times, where the condition $\Delta t_i\ll\omega_n^{-1}$ is not fulfilled, additional data points are generated by linear interpolation. It turns out that just as in the TPC experiment,[14] the integrals converge after several periods. In our case, the integration was stopped after typically 1000 periods and residual oscillations were damped by averaging over the last ten periods. For an experimental curve, which covered only five orders of magnitude in time, a comparison with the spectrum, obtained by a standard FFT technique, showed no difference.

In order to check the reliability and accuracy of the method, we generated synthetic photocurrents with known trap distributions. For calculating the photocurrent, the quantities $a$ and $b$ have to be calculated exactly based on Eqs. (9) and (10) to give the spectrum $I(\omega)$ according to Eq. (11). From that spectrum, the time-dependent photocurrent can be obtained by an inverse Fourier transform. Figure 2 shows the photocurrent together with the calculated density of capture rates for the case of two discrete traps at 100 meV and 200 meV of equal density. As can be seen from the lower part of the figure, both position and density of the traps are reproduced correctly. The approximations, described by the Eqs. (16) and (17), lead to a broadening, which results in a peak width of the order of $2k_BT$.

Further checks with an exponential density of capture rates show, that also for continuous distributions of capture rates, the input distributions are reproduced correctly. Furthermore, the range of deep traps, where the limit $a\gg 1$ no longer holds, is reproduced correctly within a numerical factor of roughly 2.

## V. RESULTS AND DISCUSSION

### A. DPOP-PPV

For the substituted derivative DPOP-PPV, TOF measurements were carried out in the temperature range between 234 and 350 K. Only for hole transport transient currents could be measured. Figure 3 shows some typical TOF curves for various temperatures and electrical-field strengths. From the effective transit time $t_{Tr}$, which is in the range between 1 $\mu$s and 1 ms, the effective mobility $\mu_{eff}$ can be calculated as

$$\mu_{eff}=\frac{d^2}{t_{Tr}U} \tag{25}$$

($d$ is the sample thickness, $U$ is the applied voltage). For times faster than $10^{-8}$ s the time dependence of the photocurrent is determined by the rise time of the experimental setup.

The effective mobility $\mu_{eff}$, as obtained by evaluating the experimental data with Eq. (25), is thermally activated with a field-dependent activation energy, as is depicted in Fig. 4. In the inset, the extrapolated least-square fits for the different electrical fields are shown. The region of

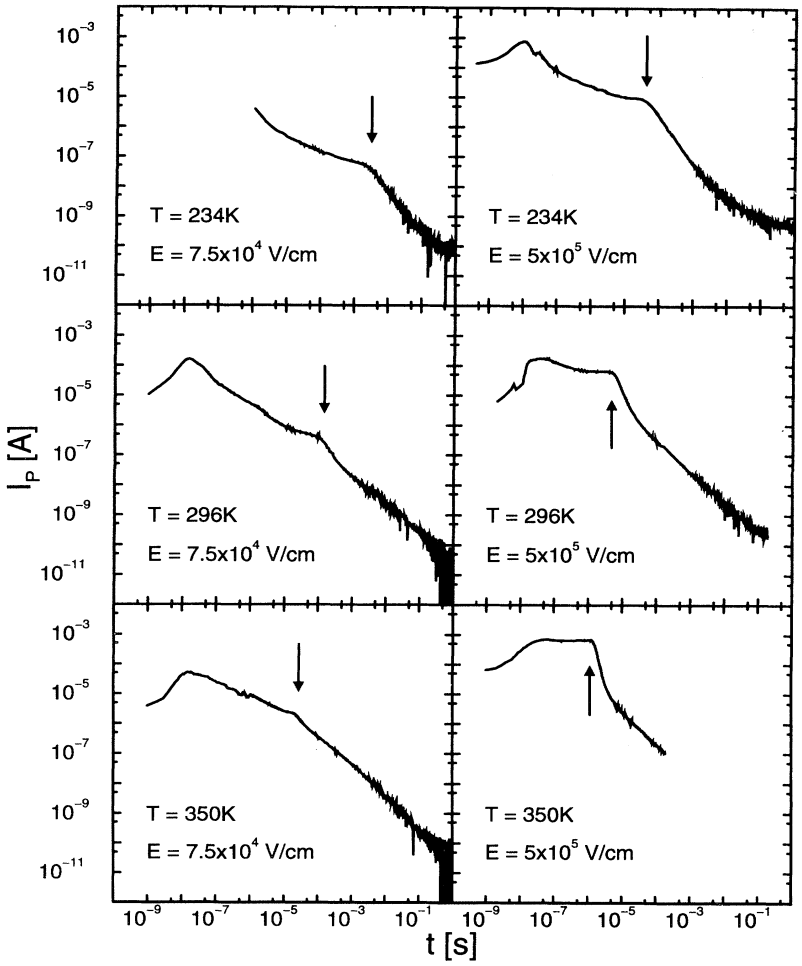


FIG. 3. DPOP-PPV: photocurrents for different temperatures and electrical fields, $d=4$ $\mu$m. The transit times $t_{\mathrm{Tr}}$ are marked with arrows.

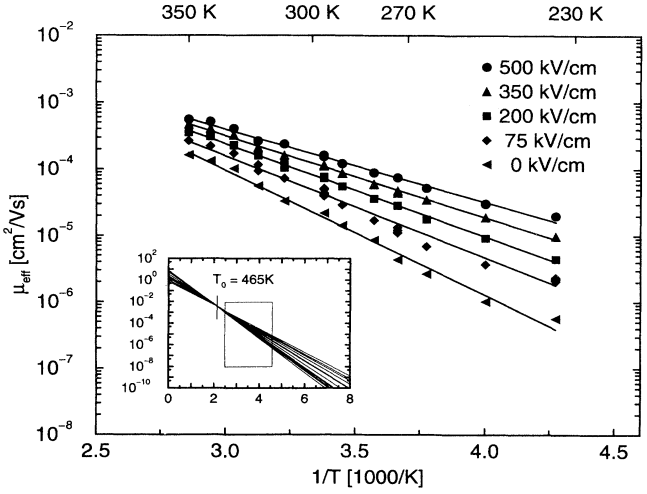


FIG. 4. DPOP-PPV (large frame): effective mobility $\mu_{\mathrm{eff}}$ as a function of temperature for some electrical fields, data points for zero field extrapolated from field-dependent measurements; inset: Arrhenius fits for different electrical fields; for details, see text.

the large frame is marked by the rectangle, drawn into the inset. It can be seen that the straight lines intersect at a characteristic temperature $T_0=465$ K. The absolute values of $\mu_{\mathrm{eff}}$ are, at room temperature, in the range of $10^{-4}$ cm$^{-2}$/V s, which is comparable with the results of Gailberger and Bässler[19] in the differently substituted derivative poly(2-phenyl-1,4-phenylene vinylene) (PPPV).

Mobility data for $E=0$ are also included in the figure. These were obtained by extrapolating the field-dependent mobility data to zero field, assuming the common, Poole-Frenkel-like, field dependence of the form

$$\log \mu_{\mathrm{eff}} \propto \mathrm{const} \times \sqrt{E} \ . \tag{26}$$

Such a field dependence has been observed for a wide variety of organic photoconductors (e.g., Refs. 16 and 20–28). Formally the temperature dependence of the measured mobilities can be described as

$$\mu_{\mathrm{eff}}=\mu_0 \exp\left[\frac{\epsilon_{\mathrm{act}}(E)}{k_B T_{\mathrm{eff}}}\right] , \tag{27}$$

with a field-dependent activation energy $\epsilon_{\mathrm{act}}(E)$

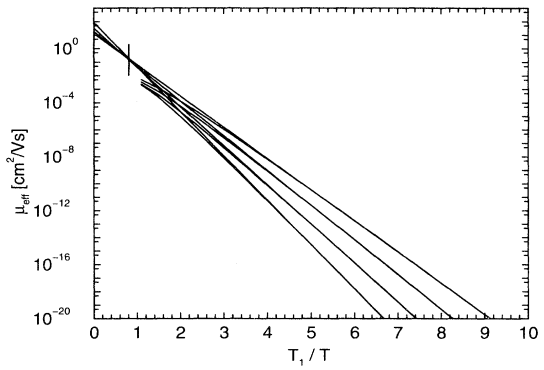


FIG. 5. Effective mobility $\mu_{\text{eff}}$, calculated according to Eq. (32) as a function of reciprocal temperature $T_1/T$ for some electrical fields; $d=4$ $\mu$m, $T_1=465$ K, $a_{\text{ges}}=10^4$, $\beta=2.08\times10^{-4}e\sqrt{\text{V cm}}$, $r_0=10^{10}$ Hz, $\epsilon_{\max}=367$ meV; for details, see text.

$=\epsilon_{\text{act}}(0)-\beta\sqrt{E}$. The effective temperature $T_{\text{eff}}$ is related to the temperature $T$, at which the experiment has been performed, by the relation

$$\frac{1}{T_{\text{eff}}}=\frac{1}{T}-\frac{1}{T_0}\ , \tag{28}$$

with an empirical characteristic temperature $T_0$. Such a temperature dependence has been published first by Gill[20] and has since been observed by several authors (e.g., Refs. 21 and 29–32).

The transit time of a charge carrier is determined by the Boltzmann activated release times from the traps. Compared to this time, the time, where the charge carrier is in highly mobile, delocalized states, can be neglected. The release time for a charge carrier from a given trap of depth $\epsilon_i$, is proportional to $\exp(\epsilon_i/k_BT)$. Assuming an exponential density of states with a decay constant of $k_BT_1$, the total time, which a carrier spends in traps with depths around $\epsilon_i$, is proportional to $\exp(\epsilon_i/k_BT)\exp(-\epsilon_i/k_BT_1)$. In the low-temperature regime ($T<T_1$), the total time, which is spent in a trap of depth $\epsilon_i$, is increasing exponentially with $\epsilon_i$. Thus, the transit time is mainly determined by the deepest traps. If a cutoff energy exists, where the density of states drops considerably faster than $\exp(-\epsilon/k_BT)$, the transit time will be approximately equal to the total time, which the carrier has spent in traps around this cutoff energy. Therefore, the activation energy for the charge-carrier transport should be equal to this cutoff energy.

The existence of a characteristic temperature $T_0$,

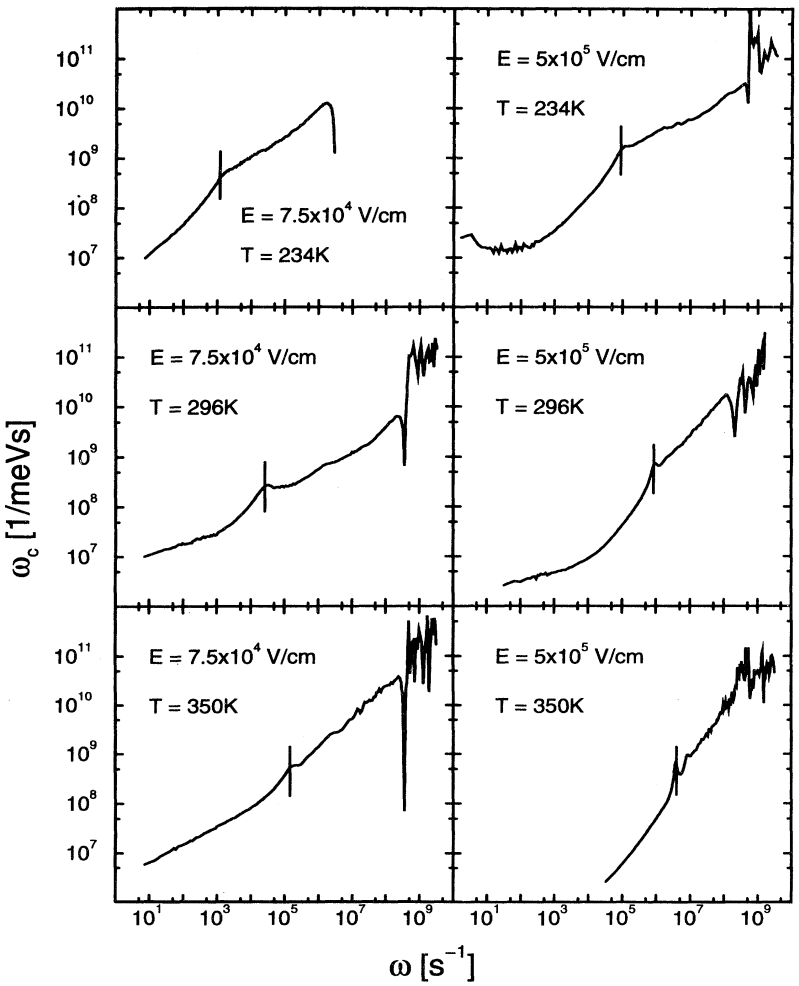


FIG. 6. DPOP-PPV: density of capture rates $\omega_c$ as a function of frequency for different temperatures and electrical fields; critical rate $r_c$ denoted by vertical bars.

where the field dependence of the effective mobility vanishes, can be understood as follows. For the case of an exponential trap distribution with a cutoff energy $\epsilon_{\max}$,

$$\rho(\epsilon,E)\propto\exp\left[-\frac{\epsilon+\beta\sqrt{E}}{k_BT_1}\right] \tag{29}$$

for $\epsilon<\epsilon_{\max}$, the transit time can be calculated to be

$$t_{\mathrm{Tr}}=\int_{-\beta\sqrt{E}}^{\epsilon_{\max}-\beta\sqrt{E}}\rho(\epsilon,E)t(\epsilon)d\epsilon\ . \tag{30}$$

The release time $t(\epsilon)$ from a trap of depth $\epsilon$ is assumed to be

$$t(\epsilon)=\frac{1}{r_0}\begin{cases}\exp\dfrac{\epsilon}{k_BT}\ , & \epsilon>0\\ 1\ , & \epsilon<0\ .\end{cases} \tag{31}$$

Here, it has been simply assumed, that all trap depths are reduced by the external field by an amount of $\beta\sqrt{E}$. From Eqs. (25), (30), and (31), the effective mobility can be calculated as

$$\mu_{\mathrm{eff}}=\frac{dr_0}{a_{\mathrm{ges}}}\frac{x-1}{E}\frac{\exp\left[\dfrac{\beta\sqrt{E}}{k_BT_1}\right]}{\exp\left[\dfrac{\epsilon_{\max}-\beta\sqrt{E}}{k_BT_1}(x-1)\right]-x}\ , \tag{32}$$

with $x=T_1/T$ ($d$ is the sample thickness, $r_0$ is the attempt-to-escape frequency, $a_{\mathrm{ges}}$ is the total number of trapping events). In Fig. 5, the effective mobility, which has been calculated according to Eq. (32), is plotted for different electrical fields with typical experimental parameters ($a_{\mathrm{ges}}=10^4$, $\beta=2.08\times10^{-4}e\sqrt{\mathrm{V\,cm}}$, $\epsilon_{\mathrm{act}}=367$ meV, $r_0=10^{10}$ Hz, $d=4$ $\mu$m, $T_1=465$ K). The dotted lines are Arrhenius fits to the low-temperature data ($x>1$). It can be seen that these fit curves intersect at $x\approx1$. Therefore, the decay constant of the trap distribution $T_1$ can be correlated with the characteristic temperature $T_0$ of Eq. (28), whereas the zero-field activation energy can be identified with $\epsilon_{\max}$.

By extrapolating the effective mobility to infinitely high temperatures ($1/T\rightarrow0$), the microscopic transit time $t_{\mathrm{mic}}$ can be obtained from the following equation:

$$t_{\mathrm{mic}}=\frac{d}{\mu(1/T\rightarrow0)E}\ . \tag{33}$$

A fit to the experimental data gives a value of $t_{\mathrm{mic}}=(7.5\pm0.6)10^{-10}$ s. With the aid of the parameter $t_{\mathrm{mic}}$, the density of capture rates $\omega_c$ can be calculated as a function of $\omega$, which is, according to Eq. (19), identical to the inverse release time. The total charge $Q_{\mathrm{ges}}$ is obtained by integrating the photocurrent over time.

Figure 6 shows the calculated density of capture rates $\omega_c$ for those photocurrents, which are displayed in Fig. 3. In all the plots, a distinct feature, which will in the following be referred to as the critical rate $r_c$, is marked by a vertical bar.

In Fig. 7, the critical rate $r_c$ is plotted for different electrical fields as a function of $1/T$. Like in Fig. 4, the inset

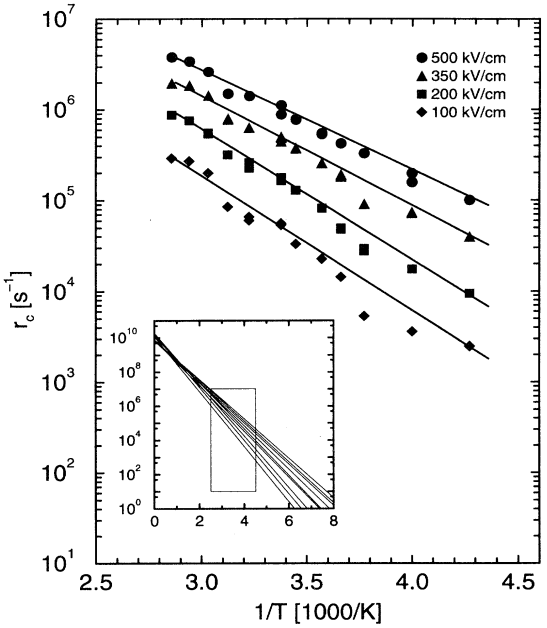


FIG. 7. DPOP-PPV: critical rate $r_c$ as a function of temperature for some electrical fields; inset: Arrhenius fits for different electrical fields; for details, see text.

shows again the least-square fits extrapolated to $1/T\rightarrow0$. The rectangle in the inset depicts the range of the large frame. The critical rate $r_c$ is thermally activated and in contrast to the data for the effective mobility, the fit curves intersect within experimental errors at $1/T=0$. This behavior is consistent with the assumption of a single, field independent, attempt-to-escape frequency $r_0$ in Eq. (13). From Fig. 7, $r_0$ can be calculated to be $r_0=(10.0\pm1.5)10^{-10}\,\mathrm{s}^{-1}$.

From the slopes of the fit curves, the activation energies for both, the critical rate $r_c$ and the effective mobility $\mu_{\mathrm{eff}}$ can be calculated. Figure 8 shows both energies as a function of the square root of the electrical field. It can be seen that within the experimental error both energies are almost identical for a given field strength. This

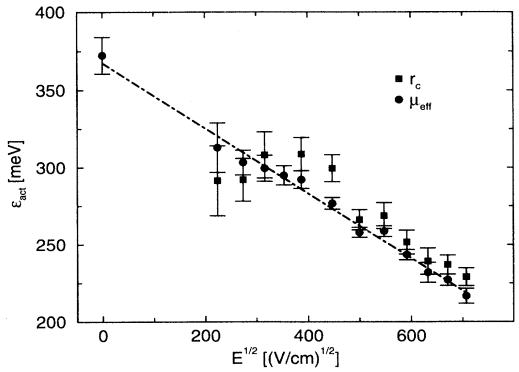


FIG. 8. DPOP-PPV: activation energy for effective mobility $\mu_{\mathrm{eff}}$ and critical rate $r_c$ as a function of electrical field. The fit curve corresponds to $\epsilon_{\mathrm{act}}(E)=\epsilon_{\mathrm{act}}(0)-\beta\sqrt{E}$, and $\epsilon_{\mathrm{act}}(0)=367$ meV and $\beta=2.08\times10^{-4}e\sqrt{\mathrm{V\,cm}}$.

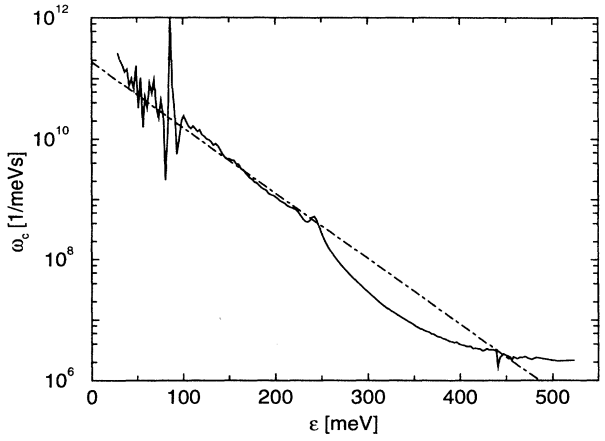


FIG. 9. DPOP-PPV (full line): calculated density of capture rates as a function of trap depth, $E=4.5\times10^5$ V/cm, $T=296$ K; dotted line: exponential trap distribution with a decay constant of 40 meV; for details, see text.

behavior will be discussed later in this section.

Figure 9 shows a typical trap distribution for DPOP-PPV. Here, the abscissa has been rescaled in energy units with the help of Eq. (13) and with $r_0=10^{10}\ s^{-1}$. It can be seen that the trap distribution is exponential between 100 meV and approximately 225 meV. The large numerical noise for energies less than 100 meV stems from the fact that these shallow traps affect the experimental data only at high frequencies or short times, where the time dependence of the photocurrent is limited by the time resolution of the experimental setup. The decay for traps deeper than approximately 225 meV is limited by the finite-energy resolution of the numerical analysis.

A dotted line is drawn into Fig. 9, which corresponds to an exponential trap density with a decay constant of 40 meV. The latter is equivalent to a characteristic temperature of $T_0=465$ K, as is consistent with the temperature dependence of the effective mobility (see Fig. 4).

By integrating the density of capture rates over the trap depths, the number of trapping events $a$ can be obtained. Figure 10 shows the quantity $a(\epsilon)$, which is

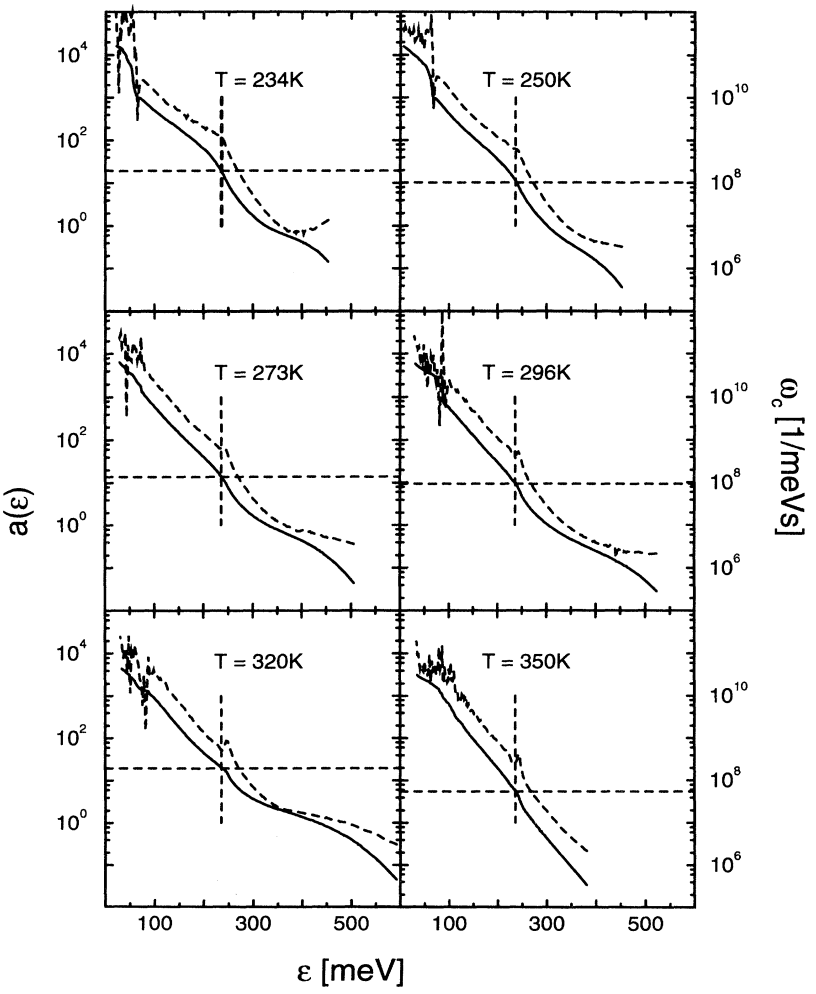


FIG. 10. DPOP-PPV (full lines and left scale): number of trapping events $a(\epsilon)$ in traps deeper than $\epsilon$; dashed lines and right scale: density of capture rates $\omega_c$; $E=4.5\times10^5$ V/cm, $t_{mic}=7.5\times10^{-10}$ s; vertical bars: critical energy $\epsilon_c=k_BT\ \ln(r_0/r_c)$; horizontal bars: $a(\epsilon=\epsilon_c)$; for details, see text.

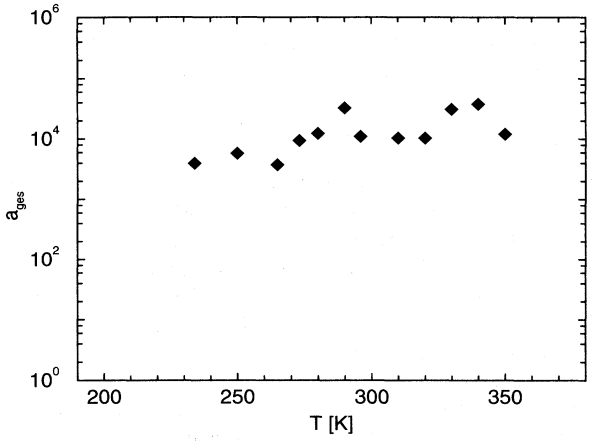


FIG. 11. DPOP-PPV: total number of trapping events $a_{ges}$ for different temperatures, $E=4.5\times10^5$ V/cm.

equivalent to $a(\omega)$ in Eq. (16). This quantity represents the total number of trapping events, which a charge carrier experiences in traps deeper than $\epsilon$ during the transit. The horizontal bars indicate, how often a charge carrier is trapped in traps deeper than the critical energy $\epsilon_c$, which is identical with the activation energy of both the critical rate $r_c$ and the effective mobility $\mu_{\text{eff}}$. It can be seen that $a(\epsilon_0)$ is roughly of the order of 10. In a qualitative picture, this means that the activation energy is determined by those traps, which are visited only a few times during the transit. A more detailed analysis shows that the transit time for all curves is roughly five times larger than the release time $r_c^{-1}$ from a trap at $\epsilon=\epsilon_c$. This behavior also shows that the transport properties are determined by the deepest traps, which are visited at least a few times during the transit, as has been postulated theoretically.[15]

If $a(\epsilon)$ is extrapolated to $\epsilon=0$, the total number of capture events $a_{ges}$ is obtained. Due to the limited time resolution of the experimental setup, the energy range with energies less than 100 meV cannot be taken into account, because these energies correspond to release rates $\omega>10^8$ s$^{-1}$. Therefore, the region between 100 and 220 meV has been extrapolated linearly in the logarithmic plot to 0 meV to obtain the total number of trapping events $a_{ges}$ as given in Fig. 11. It can be seen that a charge carrier is trapped $10^4$ times during the transit. This means that with a sample thickness of 4 $\mu$m, the charge carrier travels on the average a distance of 4 Å between two consecutive trapping events in the direction of the electrical field. Compared to this value, the spatial extension of a charged excitation in PPV along the chain has been deduced from electrochemical doping,[33–35] as well as theoretical calculations[36] to be 26. . .40 Å. This means that the component of the mean displacement per hop $d_{\text{mic}}$, which is parallel to the electrical field, is smaller than the typical extension of the excitation along the polymer backbone. This result becomes plausible with the assumption that, due to the preparation procedure, the polymer chains are partly aligned parallel to the film surface. Therefore, the transport occurs predominantly perpendicular to the chains. In stretch aligned PPV, the typical distance between two adjacent chains has been found to be 6. . .8 Å (Ref. 37) and agrees with $d_{\text{mic}}$ within a factor of 2. Since the estimated error of $a_{ges}$ is of the same order and since no corrections have been made for the three-dimensional nature of the transport, these discrepancies are not significant. From the above rough estimates, it can be concluded that in DPOP-PPV almost every monomer acts as a trap.

With Eq. (3), the quasi-Fermi-level $\epsilon_{fp}$ can be determined, if the density of states at the mobility edge $N_c$ is known. It can be estimated from $r_0=N_c v_{\text{mic}}\sigma$ to be $N_c\approx10^{19}$ cm$^{-3}$. Here, the microscopic velocity $v_{\text{mic}}$ has been calculated from $v_{\text{mic}}=d/t_{\text{mic}}=4\ \mu\text{m}/7.5\times10^{-10}$ s and the capture cross section $\sigma$ has been assumed to be $\sigma=4\times4$ Å$^2$. In a TOF experiment, $\epsilon_{fp}$ is determined by the dark current. With typical parameters (dark current $I_d=1$ nA, sample volume $V=4\times10^{-4}\times1.2\times0.3$ cm$^3$), the quasi-Fermi-level at room temperature can be estimated from Eq. (3) to be $\epsilon_{fp}\approx830$ meV. Here, the number of charges $p_0$ has been calculated from $p_0=I_d t_{\text{mic}}/e$. Assuming that the intrinsic Fermi level lies at midgap, which corresponds to 1.5 eV (band gap 3 eV), the quasi-Fermi-level is shifted towards the band edge by 670 meV. It has been pointed out in the discussion above that those traps, which determine the transport properties, have depths less than 400 meV. Therefore, trap filling effects, due to the dark current, can be neglected in DPOP-PPV.

A rough estimate can also be made for the effect of trap filling, which is caused by the photogenerated charges. With typical parameters (total photogenerated charge $Q_{ges}=3$ nC, penetration depth of the laser pulse $\delta=200$ nm), the maximum concentration of charge carriers per monomer can be calculated to be of the order of $10^{-6}$. Here, a charge carrier concentration, which decreases exponentially with the distance from the illuminated electrode, has been assumed. If all charge carriers were trapped in the lowest lying states, all states, for which $a(\epsilon)<10^4\times10^{-6}=10^{-2}$ holds, would be occupied, whereas all shallower traps would be empty. From Fig. 10, it can be seen that this estimate corresponds to traps deeper than 500 meV, which do not affect the measured transport properties.

### B. Comparison with PPV

Before comparing two different materials like PPV and DPOP-PPV, it has to be stated that mobility data for organic photoconductors depend upon the details of the chemical synthesis and the sample preparation. Therefore, they differ by factors of typically 2 or 3, when data for nominally identical samples are compared, which were measured by different groups, whereas the values for quantities like the activation energy normally differ by 20% or less. As will be shown in this subsection, however, the differences for the mobility data between PPV and DPOP-PPV are four orders of magnitude and cannot be accounted for by details of the sample preparation.

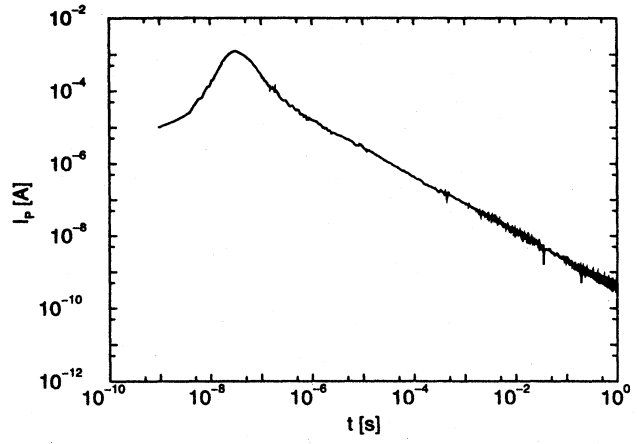


FIG. 12. PPV: photocurrent at $T=400$ K, sample thickness $d=7$ $\mu$m, $E=2.5\times10^5$ V/cm.

In contrast to DPOP-PPV, the charge-carrier transport in PPV is completely dispersive. Even at a temperature of 400 K, the photocurrent for holes shows a featureless decay without a discernible transit time (see Fig. 12). As mentioned in Sec. II already, no changes were found after variation of both the elimination conditions and the conditions of the heat treatment prior to the measurements.

Since no transit time can be detected in PPV, it is not possible to measure the effective mobility directly by a TOF experiment. Additionally, the attempt-to-escape frequency $r_0$ cannot be determined, and thus it is impossible to calculate trap depths from the release rates $\omega$. Figure 13, therefore, shows only the quantity $a(\omega)$ as a function of release rates $\omega$ both for PPV and for DPOP-PPV. As a guide for the eye, the horizontal bar indicates where $a(\omega)$ reaches the value of one.

With these data, however, an indirect estimate of the effective mobility for holes in PPV can be made. As mentioned earlier, the traps, which determine the transport properties, are those where $a(\epsilon)$ or $a(\omega)$ are of the order of 1...10. In DPOP-PPV, the transit time is of the same order of magnitude as the corresponding release time $\omega^{-1}$ ($\omega=r_c$). Therefore, $\omega^{-1}$ ($a=1$) is a good measure for the transit time $t_{\mathrm{Tr}}$. It can be seen in Fig. 13 that this time, which is between $10^{-6}$ and $10^{-4}$ s in DPOP-PPV, extrapolates as being longer than $10^{-1}$ s in PPV. Since $a(\omega)$ has been obtained by integrating the density of cap-

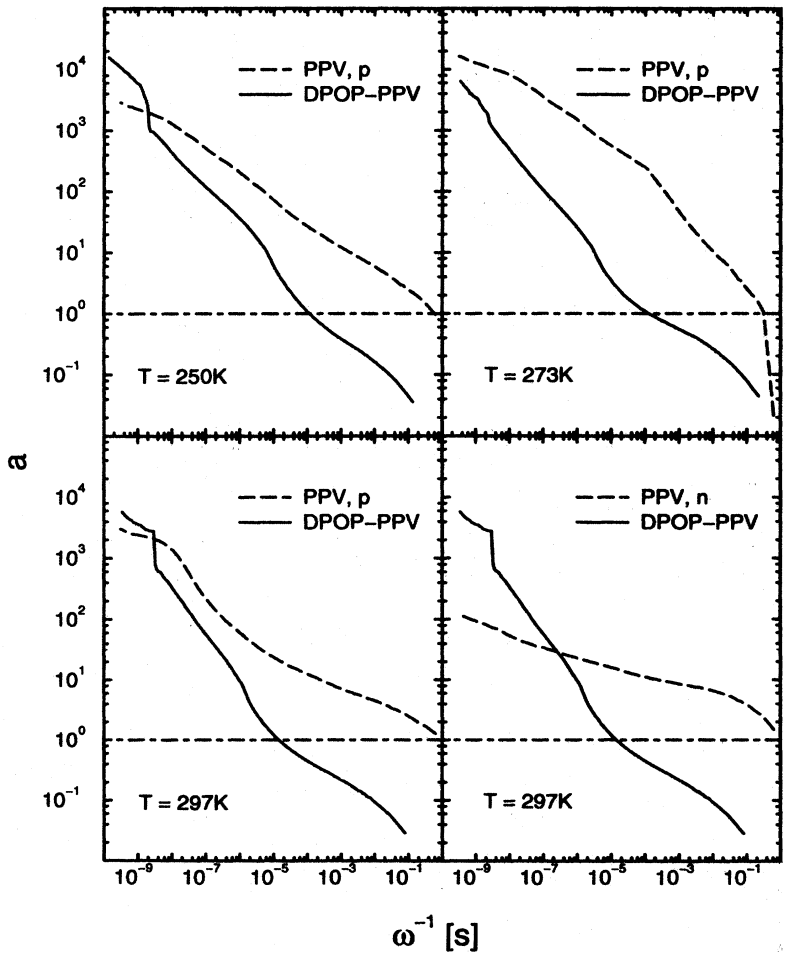


FIG. 13. Total number of capture events: comparison between PPV (dashed lines) and DPOP-PPV (full lines) for different temperatures; DPOP-PPV: hole transport, PPV; $p$ is the hole transport, PPV; $n$ is the electron transport; $E=4.5\times10^5$ V/cm.

ture rates over release rates, beginning at low release rates, the value of $10^{-1}$ s is a lower limit only. From this time, an upper limit for the effective mobility of PPV can be deduced to be $\mu_{\text{eff}} < 1.5 \times 10^{-8}$ cm$^2$/V s (sample thickness $d = 7$ $\mu$m).

By extrapolating $a(\omega)$ to the ordinate and neglecting again the region with $\omega < 10^{-8}$ s, it can be seen that in all curves, except for electron transport, the total number of capture events is roughly $10^4$ for both materials. Therefore, the poor transport properties of PPV compared to DPOP-PPV are not due to the fact that in PPV, the density of traps is higher than in DPOP-PPV. It is rather caused by the fact that the release times of those traps, which determine the transport properties, are more than four orders of magnitude slower as compared to those in DPOP-PPV.

Assuming an attempt-to-escape frequency $r_0 = 10^{10}$ s$^{-1}$ for PPV also, a release rate of $10^{-1}$ s corresponds to a trap depth of roughly 600 meV. This value is in good agreement with the data from thermally stimulated current (TSC) experiments.[38] Onoda, Park, and Yoshino[38] found two peaks $P_1$ and $P_2$ in the TSC spectrum, which correspond to trap depths of 360 meV ($P_1$) and 550 meV ($P_2$), respectively. For samples with elimination temperatures above 530 K, the amplitude of $P_1$ is lowered significantly. This feature and the fact, that $P_1$ is sensitive to $I_2$ doping, is interpreted by Onoda, Park, and Yoshino[38] in terms of doping related impurities. Due to the chemical synthesis from a water soluble salt, the existence of charged impurities has to be expected in partly eliminated PPV. By raising the elimination temperature, elimination is improved, as can be seen by elemental analysis (see Sec. II). Therefore $P_1$ should be lowered by improving the elimination. This finding is consistent with the fact that $P_1$ is much less pronounced in thin samples ($d = 5$ $\mu$m), as compared to thick samples ($d = 20$ $\mu$m), because in thin samples, the elimination process should be faster under identical conditions.[38] With $r_0 = 10^{10}$ s$^{-1}$, the trap depth of $P_1$ corresponds to a release time of roughly 200 $\mu$s. Since we used thin samples ($d = 7$ $\mu$m), which were eliminated at temperatures above 530 K, we do not observe this feature in our data (see Fig. 13).

The amplitude of $P_2$ is lowered drastically after stretch alignment of the samples.[38] Therefore, the defects related with $P_2$, can be either located in the amorphous parts of the samples or can be related to the partly crystalline nature of PPV.[39] Since grain boundaries form extremely efficient traps in organic photoconductors,[40] we think that the dispersive nature of the charge-carrier transport in PPV is, most likely, due to the existence of grain boundaries, although chemical impurities cannot be ruled out completely. In the case of DPOP-PPV, it can be assumed that the bulky substituents inhibit crystallization. Therefore, the absence of grain boundaries would account for the enhanced transport properties as compared to PPV, although the three-dimensional interchain coupling, which is necessary for charge transport over macroscopic distances, should be reduced by the substituents.

In contrast to DPOP-PPV, electron transport is also found in PPV. The estimated quantum efficiency, however, is roughly ten times smaller than the quantum efficiency for holes. Obviously, the *schubweg* for electrons is considerably smaller than the one for holes, or in other words, electrons are trapped within the bulk material for a time, which is longer than the experimental time range of 10 s. This consideration is consistent with the finding that for electrons, the calculated total number of trapping events is much smaller than the comparable figure for hole transport. From Fig. 13, a value of $a_{\text{ges}} \approx 200$ can be estimated.

This asymmetry between hole transport and electron transport is in qualitative agreement with the data obtained with different methods from Antoniadis, Abkowitz, and Hsieh.[41] They determined the deep-trapping mobility-lifetime product $\mu\tau$ in PPV with charge collection experiments and found $\mu\tau = 10^{-9}$ cm$^2$/V for holes and $\mu\tau = 10^{-12}$ cm$^2$/V for electrons. Within the scope of this work, the detailed microscopic origin for this asymmetry cannot be determined, however.

## VI. SUMMARY

We characterized the charge transport properties of DPOP-PPV and PPV by TOF measurements. It has been found that hole transport in DPOP-PPV can be consistently described within the framework of a conventional multiple trapping picture.

A numerical approach has been described to calculate the density of localized states from the measured photocurrent with the multiple trapping model. As a result, hole transport in DPOP-PPV can be well described with an exponential density of localized states up to a well-defined critical energy, where the density of states drops sharply. It has been found that this energy is identical with the measured activation energy of the effective mobility.

From the total number of trapping events, the mean distance, which a charge-carrier travels parallel to the electrical field between two trapping events, can be estimated to be of the order of 4 Å. This value is comparable to the distance between two adjacent polymer chains. In particular, the overall density of traps is comparable to the density of monomer units, indicating that in real samples, there is no charge-carrier transport in bandlike states over distances, which are much longer than the extension of a monomer unit. It can, therefore, be concluded, that the transport in the conjugated polymer DPOP-PPV occurs by a conventional hopping mechanism.

The transport properties of PPV are completely dispersive. It is, therefore, impossible to obtain mobility data directly by TOF experiments. By comparison with the data for DPOP-PPV, it can be seen that this dispersive behavior is due to the fact that in PPV, the release times from those traps, which determine the transport properties, are typically more than three orders of magnitude longer than comparable release times in DPOP-PPV. Even at room temperature they reach typical values of more than $10^{-1}$ s. We attribute this behavior to the existence of grain boundaries in PPV.

## ACKNOWLEDGMENTS

This work was supported by the Fonds der Chemischen Industrie and the Sonderforschungsbereich 213. The authors would like to thank M. Schwoerer and W. Rieβ for stimulating discussions and J. Gmeiner and P. Strohriegl for providing the PPV precursor polymer.

[1]A. J. Heeger, S. Kivelson, J. R. Schrieffer, and W.-P. Su, Rev. Mod. Phys. **60**, 781 (1988).
[2]*Conjugated Polymers,* edited by J. L. Brédas and R. Silbey (Kluwer, Dordrecht, 1991).
[3]J. H. Burroughes, D. D. C. Bradley, A. R. Brown, R. N. Marks, K. Mackay, R. H. Friend, P. L. Burns, and A. B. Holmes, Nature **347**, 539 (1990).
[4]G. Gustafsson, Y. Cao, G. M. Treacy, F. Klavetter, N. Colaneri, and A. J. Heeger, Nature **357**, 477 (1992).
[5]A. R. Brown, D. D. C. Bradley, J. H. Burroughes, R. H. Friend, N. N. Greenham, P. L. Burn, A. B. Holmes, and A. Kraft, Appl. Phys. Lett. **61**, 2793 (1992).
[6]C. Zhang, D. Braun, and A. J. Heeger, J. Appl. Phys. **73**, 5177 (1993).
[7]S. Karg, W. Riess, V. Dyakonov, and M. Schwoerer, Synth. Met. **54**, 427 (1993).
[8]I. Sokolik, Z. Yang, F. E. Karasz, and D. C. Morton, J. Appl. Phys. **74**, 3584 (1993).
[9]A. Kraft, P. L. Burn, A. B. Holmes, D. D. C. Bradley, A. R. Brown, R. H. Friend, and R. W. Gymer, Synth. Met. **55**, 936 (1993).
[10]H. Domes, R. Fischer, D. Haarer, and P. Strohriegl, Makromol. Chem. **190**, 165 (1989).
[11]J. Gmeiner, S. Karg, M. Meier, W. Rieβ, P. Strohriegl, and M. Schwoerer, Acta Polym. **44**, 201 (1993).
[12]H. Oheda, J. Appl. Phys. **52**, 6693 (1981).
[13]R. Brüggemann, C. Main, J. Berkin, and S. Reynolds, Philos. Mag. B **62**, 29 (1990).
[14]C. Main, R. Brüggemann, D. P. Webb, and S. Reynolds, Solid State Commun. **83**, 401 (1992).
[15]F. W. Schmidlin, Phys. Rev. B **16**, 2362 (1977).
[16]E. Muller-Horsche, D. Haarer, and H. Scher, Phys. Rev. B **35**, 1273 (1989).
[17]R. Pandya and E. A. Schiff, Philos. Mag. B **52**, 1075 (1985).
[18]T. Tiedje and A. Rose, Solid State Commun. **37**, 49 (1980).
[19]M. Gailberger and H. Bässler, Phys. Rev. B **44**, 8643 (1991).
[20]W. D. Gill, J. Appl. Phys. **43**, 5033 (1972).
[21]S. J. Santos Lemus and J. Hirsch, Philos. Mag. B **53**, 25 (1986).
[22]A. Peled, L. B. Schein, and D. Glatz, Phys. Rev. B **41**, 10 835 (1990).
[23]D. Haarer, H. Meyer, P. Strohriegl, and D. Naegele, Makromol. Chem. **192**, 617 (1991).
[24]P. M. Borsenberger, L. Pautmeier, and H. Bässler, J. Chem. Phys. **94**, 5447 (1991).
[25]J. Hirsch, J. Phys. C **12**, 321 (1979).
[26]M. Abkowitz and M. Stolka, Philos. Mag. Lett. **58**, 239 (1988).
[27]P. M. Borsenberger, J. Appl. Phys. **68**, 5682 (1990).
[28]D. M. Pai, J. F. Yanus, M. Stolka, D. Renfer, and W. W. Limburg, Philos. Mag. B **48**, 505 (1983).
[29]G. Pfister, Phys. Rev. B **16**, 3676 (1977).
[30]M. Stolka, J. F. Yanus, and D. M. Pai, J. Phys. Chem. **88**, 4707 (1984).
[31]R. Oshima, T. Uryu, and M. Seno, Macromolecules **18**, 1043 (1985).
[32]M. A. Abkowitz, M. J. Rice, and M. Stolka, Philos. Mag. B **61**, 25 (1990).
[33]J. B. Schlenoff, J. Obrzut, and F. E. Karasz, Phys. Rev. B **40**, 11 822 (1989).
[34]J. Obrzut and F. E. Karasz, J. Chem. Phys. **87**, 6178 (1987).
[35]J. Obrzut and F. E. Karasz, J. Chem. Phys. **87**, 2349 (1987).
[36]H. Eckhardt, R. H. Baughman, J. P. Buisson, S. Lefrant, C. X. Cui, and M. Kertesz, Synth. Met. **43**, 3413 (1991).
[37]T. Garnier, E. L. Thomas, D. R. Gagnon, F. E. Karasz, and R. W. Lenz, J. Polym. Sci. B Polym. Phys. Ed. **24**, 2793 (1986).
[38]M. Onoda, D. H. Park, and K. Yoshino, J. Phys. (London), Condens. Matter **1**, 113 (1989).
[39]D. D. C. Bradley, T. Hartmann, R. H. Friend, E. A. Marseglia, H. Lindenberger, and S. Roth, in *Electronic Properties of Conjugated Polymers,* edited by H. Kuzmany, M. Mehring, and S. Roth, Springer Series in Solid-State Sciences Vol. 76 (Springer-Verlag, Berlin, 1987), p. 308.
[40]D. Adam, F. Closs, T. Frey, D. Funhoff, D. Haarer, H. Ringsdorf, P. Schuhmacher, and K. Siemensmeyer, Phys. Rev. Lett. **70**, 457 (1993).
[41]H. Antoniadis, M. A. Abkowitz, and B. R. Hsieh, Appl. Phys. Lett. **65**, 2030 (1994).